ELSEVIER

Composite Structures 45 (1999) 13–27

COMPOSITE STRUCTURES

Buckling of woven GFRP cylinders under concentric and eccentric compression

A.Y. Elghazouli, M.K. Chryssanthopoulos, I.E. Esong

Department of Civil Engineering, Imperial College of Science, Technology and Medicine, London SW7 2BU, UK

Abstract

The experimental behaviour of laminated glass fibre-reinforced plastic (GFRP) cylinders under compression and bending is examined in this paper. The laminates are of type 'Rovimat 1200' consisting of woven glass fibre roving, with a chopped mat on one side, within a polyester resin matrix. Two and three-ply cylinders with various orthogonal orientations were considered, for which the nominal radius-to-thickness ratio was about 108 and 72, respectively. Use was made of an automated laser scanning system for measuring geometric imperfections and progressive buckling deformations of the models. Following a description of the specimen and loading details, the results of experiments on ten models are presented. The results include thickness and imperfection mapping, displacement and load measurements as well as important observations regarding the failure mode and overall behaviour of each model. The findings highlight the effects of laminate construction and loading eccentricity on the buckling strength of cylinders within the range examined. Both elastic buckling and material-dominated failure modes were observed, depending on the slenderness and load type considered. The tests also provide detailed experimental data, which are necessary for further analytical and design studies.

1. Introduction

Composite materials are being increasingly used in several applications within the civil, marine and aerospace industries. To this end, glass-reinforced plastic (GRP) shells form an attractive alternative to other materials due to their advantages in terms of the relatively low weight and cost as well as inherent corrosion-resistance. Nevertheless, the limited availability of design information, and particularly the dearth of buckling strength criteria has generally restricted the effective use of GRP shells.

Considerable developments and extensive research has been carried out over many years in order to study the shell buckling phenomenon [1,2] with emphasis on its application to isotropic materials. Early efforts were based on providing estimates of the buckling strength using semi-empirical test-based knock-down factors in conjunction with formulae for linear critical loads. In the last two decades, shell buckling tests entailed accurate measurement of input and response measurements, which are then used for validating numerical and analytical tools, hence allowing wider parametric investigations.

The use of a combined computational/experimental approach becomes essential in composite shells because of the very large number of variables involved which prohibits a purely experimental approach. These variables include basic lamina properties, number, and orientations in addition to the same geometric and load parameters associated with homogeneous shells. To enable adequate calibration and validation of analytical models, it is imperative that detailed measurement of salient parameters is undertaken prior to and during testing. In particular, due to the long recognised [3,4] imperfection sensitivity of shells subjected to axial compression, mapping of initial geometric imperfections requires specific attention.

In the area of composite shells, several studies have been carried out to investigate the experimental and analytical buckling response of cylinders [5–7]. However, in most investigations dealing with laminated cylinders, the models are extremely thin-walled and usually made of graphite-epoxy systems, since the intended applications lie largely in the aeronautic industry. Comparatively, only few glass-fibre shells have been tested, and results reported do not enable analytical and numerical validation studies to be undertaken.

This paper presents the results of a series of buckling tests on laminated composite cylinders made from glass reinforced plastic (GRP) subject to concentric and eccentric compression. The study forms part of a large

0263-8223/99/$ – see front matter
PII: S0263-8223(99)00008-2

project involving detailed experimental and analytical investigations into the behaviour of composite shells. The main objectives of the tests are to provide experimental data on the interaction between buckling and material failure in GRP systems and to provide data to validate numerical tools for further parametric studies.

In this test series, ten cylinders were tested in which the ply number and orientation was varied. Three configurations of laminated cylinders were examined, namely two-ply with (0°/0°) and (0°/90°) orientation, and three-ply with (0°/90°/0°) orientation. The laminates are of type 'ROVIMAT 1200' formed from E-glass woven rovings with a chopped mat and isophthalic polyester resin. The dimensions of the cylinders were selected such that failure occurs by local shell rather than column buckling, and such that theoretically the initiation of buckling precedes material failure. For the cylinders considered, the nominal radius-to-thickness ratios were 108 and 72, for the two and three-ply models, respectively. The experimental set-up and loading arrangement are first outlined. This is followed by a detailed account of the specimen details and experimental findings, together with comparison with linear finite element analysis results.

2. Testing arrangement

The experimental set-up used for all the buckling tests is shown in Fig. 1. This arrangement enables testing under concentric as well as eccentric compressive loads. As shown in Fig. 1, the axial loading is applied through a hydraulic actuator of 1000 kN capacity operating in displacement control. A load cell and a displacement transducer are attached to the actuator piston to measure the central load and deflection, respectively.

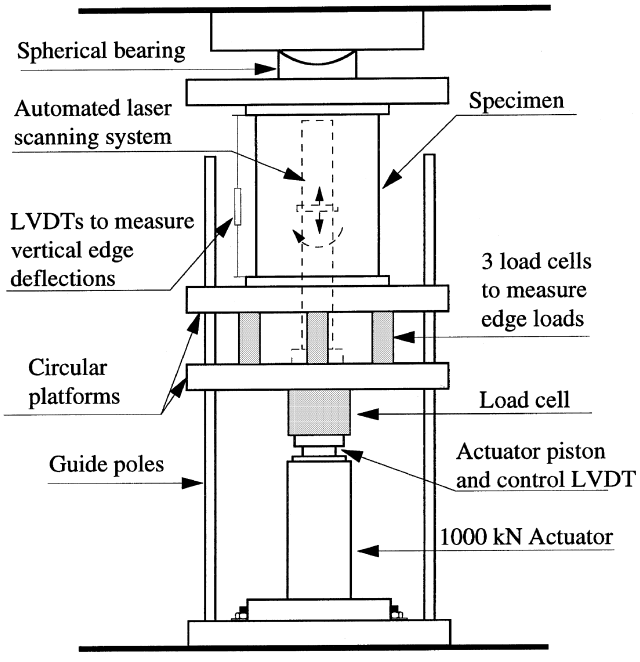

Fig. 1. Layout of test-rig.

The load from the actuator is transferred to the bottom end of the specimen through a pair of stiff circular platens which are separated by three load cells, each of 500 kN capacity, placed on spherical bearings. The cells are positioned along radii emanating from the centre of the model, each pair forming an angle of 120°. Under concentric axial compression, the three load cells should read the same value thus verifying the concentricity of applied loading. The same radial arrangement of the three load cells is also used for positioning three displacement transducers which measure the vertical deformation between the ends of the specimen.

In order to create well defined end conditions during the buckling tests, the two ends of the specimen are carefully positioned in heavy, accurately machined steel rings. The gap between the model and the rings is then filled with epoxy resin. In the test rig, the lower ring of the cylindrical specimen is clamped to the circular platen, and the top ring is connected to the top bearing through an intermediate plate. Through appropriate positioning of the top spherical bearing in relation to the cylinder axis, eccentric compressive loading can be generated. The load is reacted against two parallel reaction frames, each consisting of a stiff reaction beam rigidly connected to solid columns, which are in turn anchored to the strong floor of the laboratory.

An automated non-contact laser scanning system was used for acquiring the initial imperfections as well as the progressive change in deformations of the inner wall of the specimen during loading. This measurement system has many advantages over conventional transducer-based methods particularly in terms of accuracy, speed and non-interference with structural deformations [8].

As indicated in Fig. 1, the laser scanning system operates inside the specimen. The system allows for full circumferential and axial travel. Careful attention was given to the repeatability and accuracy of the results. Further information on the development and verification of the laser system is given elsewhere, [8]. In addition to the laser scanning, all loading and data acquisition procedures were fully automated through computer-controlled techniques.

3. Specimen and material details

The cylindrical models were produced by a specialised manufacturer (Intermarine-Tencara) from 'Rovimat 1200' Laminates using a purpose built mandrel and traditional hand lay-up. The nominal dimensions of the cylindrical models are shown in Fig. 2. All models had an internal diameter of 600 mm and an overall length of

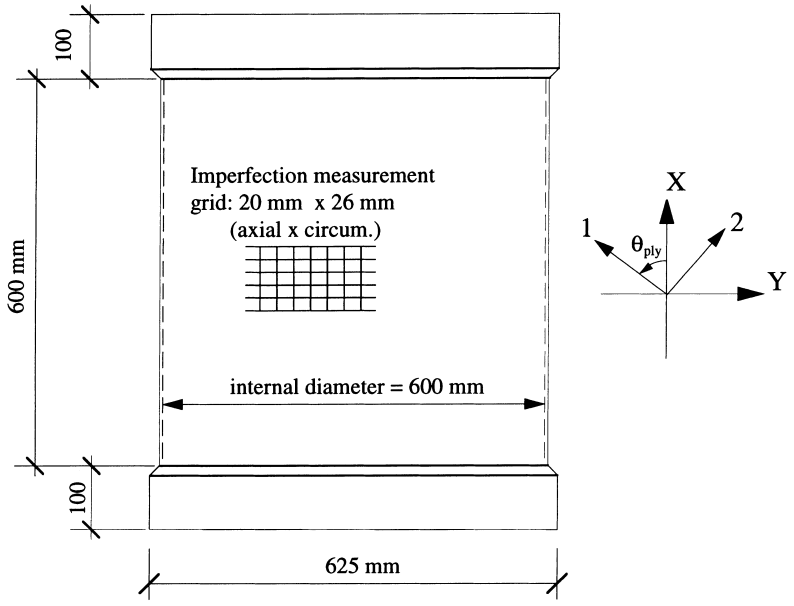

Fig. 2. Specimen geometry.

800 mm, which comprised of a central 600 mm test length and two end parts each of 100 mm length. The end parts were significantly thicker than the middle part to ensure zero radial displacements along the edges and to minimise the risk of local splitting or delamination at the boundaries.

The fibre material of the Rovimat 1200 laminate is E-glass woven roving and the resin is isophthalic polyester identified by the reference 'Synolite 0288-T-1'. The type of weave is 'SAIA 3/1', and the size of fibres is referred to as 'Silane'. The roving is sprinkled on one surface with chopped glass fibres to enhance bonding of plies. Close up views of the two faces of the roving are shown in Fig. 3. In addition to cross-weaving, the mat is stitched along the weft direction to facilitate wrapping and accurate lay-up. The nominal glass fibre volume fraction, V_f, is 33.8% and the matrix volume fraction, V_m, is about 47±0.6%. The fibres have a nominal elastic modulus of 69 GPa, nominal density of 2.5 g/m^2 and ultimate tensile strength of 2.4 GPa. The tex count roving in the warp direction is 1200 (1920/10 mm construction), and 2400 in the weft direction (2640/10 mm construction). The resin has a nominal elastic modulus of 4.0 GPa, nominal density of 1.2 g/m^2 and tensile strength of 73 MPa (ultimate tensile strain of 2.4%).

Two types of symmetric lay-up (0°/0°) and cross-ply (0°/90°/0°) laminates, both regular and balanced are used in this test series. For these two laminates, the stiffness matrices are simplified due to the uncoupled stiffnesses, particularly axial-flexural stiffness (B_{ij}, A_{16}, A_{26}, D_{16} and D_{26} terms are zero). In addition, an anti-symmetric cross-ply lay-up (0°/90°) was used, in which a degree of axial-flexural coupling is introduced (B_{11} and B_{22} are non-zero).

Mechanical property tests for the Rovimat 1200 ply (1.4 mm nominal thickness) were carried out at Politecnico di Milano [9] to the relevant ASTM standards using two-ply flat 0°/°0 (i.e. $(0)_2$) specimens and the results are reported in Table 1. In the table, directions '1' and '2' refer to the weft and warp directions of the laminate, respectively. It should be noted that the average thickness of the two-ply flat specimen was 3.1 mm which is more than 10% higher than the nominal thickness. It is also noteworthy that the elastic moduli of the laminates exhibit very similar values in tension and compression. Furthermore, the elastic moduli in both the weft and warp directions are not significantly different.

The properties of laminates of other orientations (i.e. 0°/90° and 0°/90°/0° in this study) may be estimated using classical laminate analysis. In view of the importance of mechanical properties, and the commonly-observed variation in their values, further tests were carried out [9] on flat specimens made from 0°/90° and 0°/90°/0° laminates. Additional tests were also carried out at Imperial College to confirm the material properties of core specimens extracted from the cylindrical models.

It should be noted that the values obtained will vary depending on the standard adopted and the type and dimensions of the test specimen. Close examination of the material properties with due consideration of classical laminate equations, indicates possible variations of about ±10%. This is a consequence of the sensitivity of the results to a number of factors including specimen thickness and size, testing method, resin content, etc. In particular, careful attention must be given to the effect of thickness variations in determining the effective

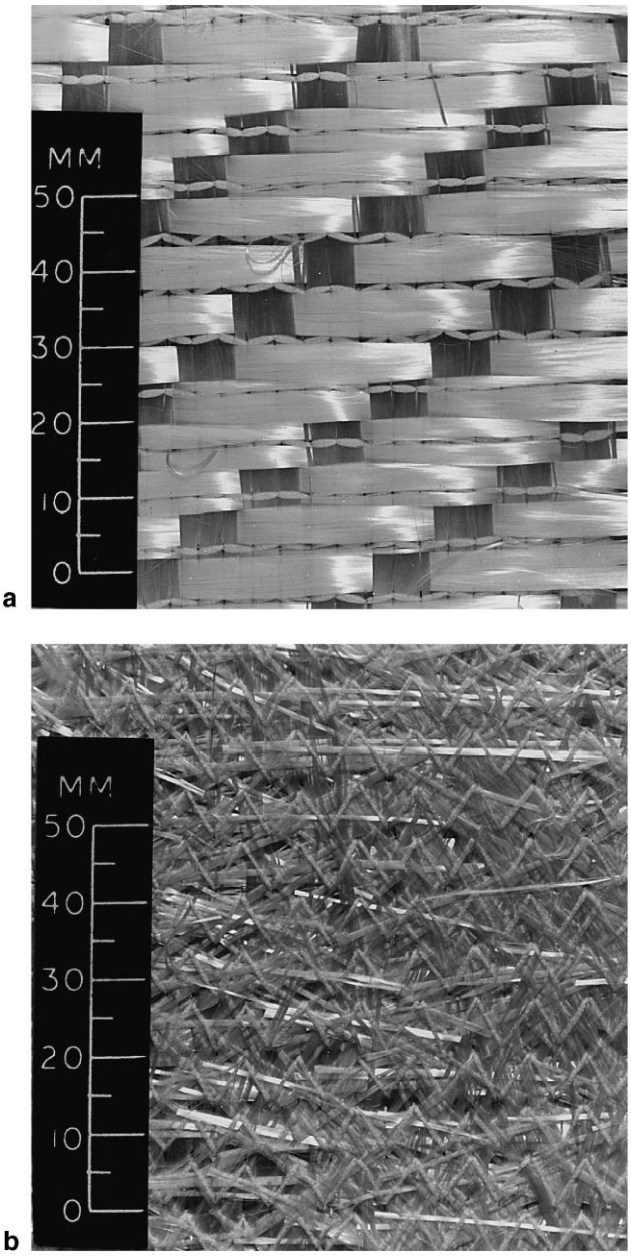

Fig. 3. View of both sides of 'Rovimat 1200' ply: (a) Woven roving (vertical : warp; horizontal : weft); (b) Chopped E-glass mat.

material properties. These aspects are discussed further in subsequent sections.

Within the series described in this paper, a total of ten cylinders were tested under concentric and eccentric compression as shown in Table 2. The table includes the specimen reference, laminate designation and orientation, total nominal thickness and nominal radius-to-thickness (r/t) ratio. The type of loading applied is also given in the table, where e/r refers to the ratio of eccentricity to cylinder radius. Direction 0° indicates that the ply is laid with the weft parallel to the axis of the cylinder. Other ply orientations may be identified through the axis system given in Fig. 2.

Table 1
Rovimat 1200 ply properties obtained from flat two-ply (0°/0°) specimens

Property	Direction	Value $[0°]_2$
Elastic Modulus (GPa) (in tension)	E_1	14.7 ± 0.1
	E_2	13.2 ± 0.4
Elastic Modulus (GPa) (in compression)	E_1	14.4 ± 0.5
	E_2	13.3 ± 0.6
Poisson's Ratio	ν_{12}	0.26 ± 0.02
Shear Modulus (GPa)	G_{12}	3.5 ± 0.1
Tensile Strength (MPa)	σ_1	199.6 ± 11.5
	σ_2	178.5 ± 7.4
Compressive Strength (MPa)	σ_1	249.6 ± 38.9
	σ_2	217.1 ± 14.3
Shear Strength (MPa)	τ_{12}	103.6 ± 7.1

As mentioned earlier, the cylinders were manufactured by hand lay-up using a specially prepared mandrel. Fig. 4 shows the details of the lay-up procedure used for the models, in which overlaps of 50 mm nominal width were used in a staggered pattern. For the 0°/0° laminates, two diametrically-opposite vertical overlaps were used. For the 0°/90° and 0°/90°/0° laminates, four vertical overlaps were used due to limitations in the roll width in the orthogonal (i.e. 90°) direction combined with the desirable symmetry about two perpendicular axes.

4. Thickness mapping

Significant thickness variations may be present in the cylindrical specimens particularly when traditional manufacturing methods, such as hand lay-up, are used. In order to measure these variations, measurement of the actual thickness of all cylinders was carried out using a grid of 50 mm × 50 mm covering the full circumference and the middle 500 mm of the specimen height. This grid was refined to 25 mm × 25 mm at the locations of overlaps, which were nominally of 50 mm width. Measurement of cylinder thickness was carried out using a vernier micrometer mounted on a specially-designed bracket.

Table 3 presents the details of the thickness measurements for all models. For each cylinder, the average thickness within each normal (N) and overlap zone (OL) is indicated together with the overall mean value for the model (excluding overlaps). The typical coefficient of variation of the thickness within a specific zone varied between 5% and 10%. Typical thickness maps for one model from each of the three laminate designations (i.e. 0°/0°, 0°/90° and 0°/90°/0°) are shown in Fig. 5. A perspective thickness map of Model RVM01 (0°/0°) is shown in Fig. 5(a) clearly depicting the position of the two overlaps (OL1 and OL2) and two normal zones (N1 and N2). Similarly, Fig. 5(b) shows the thickness pattern of one of the 0°/90° models (RVM04) in which the four

Table 2
Details of testing programme

Specimen reference	Lamination	Total nominal thickness (mm)	Nominal r/t ratio	Loading
RVM00	0°/0°	2.8	108	Concentric ($e/r = 0$)
RVM01	0°/0°	2.8	108	Concentric ($e/r = 0$)
RVM02	0°/0°	2.8	108	Eccentric ($e/r = 0.10$)
RVM03	0°/0°	2.8	108	Eccentric ($e/r = 0.25$)
RVM04	0°/90°	2.8	108	Concentric ($e/r = 0$)
RVM05	0/90°	2.8	108	Concentric ($e/r = 0$)
RVM05A	0°/90°	2.8	108	Concentric ($e/r = 0$)
RVM05B	0°/90°	2.8	108	Eccentric ($e/r = 0.25$)
RVM06	0°/90°/0°	4.2	72	Concentric ($e/r = 0$)
RVM07	0°/90°/0°	4.2	72	Concentric ($e/r = 0$)

Table 3
Measured thickness of cylindrical models

Model/zone	N1	OL1	N2	OL2	N3	OL3	N4	OL4	Mean[a]
RVM00	3.20	4.21	3.17	4.68	–	–	–	–	3.18
RVM01	3.18	4.97	3.52	4.63	–	–	–	–	3.35
RVM02	3.39	4.99	3.53	4.63	–	–	–	–	3.46
RVM03	3.38	4.76	3.47	4.76	–	–	–	–	3.42
RVM04	3.10	4.30	3.19	4.72	3.19	4.05	3.14	4.37	3.15
RVM05	3.50	4.19	3.31	4.42	3.25	4.65	3.57	4.67	3.40
RVM05A	3.13	4.58	3.34	4.00	3.20	4.21	3.13	4.17	3.20
RVM05B	3.32	4.39	3.38	4.25	3.17	4.18	3.17	4.30	3.26
RVM06	4.52	5.50	4.31	5.58	4.44	5.45	4.14	5.33	4.35
RVM07	4.72	5.76	4.82	6.58	4.80	6.06	4.80	5.24	4.78

[a]Excluding overlaps.

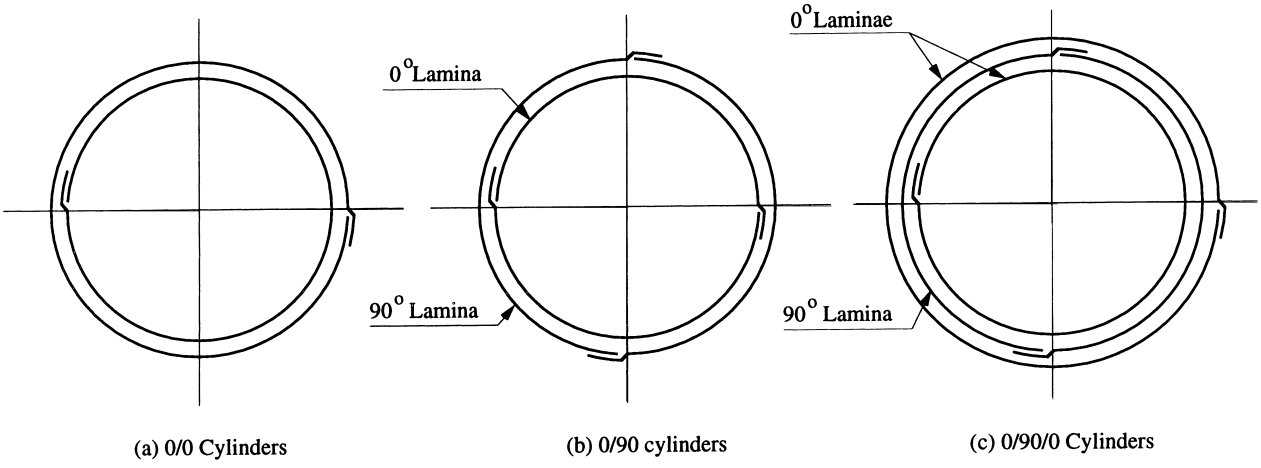

Fig. 4. Cross-section of cylinders indicating ply construction and relative position of overlaps: (a) 0°/0° cylinders; (b) 0°/90° cylinders; (c) 0°/90°/0° cylinders.

overlaps (OL1 to OL4) and the four normal zones (N1 to N4) are indicated. In Fig. 5(c), the thickness of Model RVM06 (0°/90°/0°) is depicted in which the position of the four overlaps is shown.

From the mean values shown in Table 3, it is worth noting that the measured thickness may be up to 20% higher than the nominal values in the normal zones. Since these values do not include any overlaps, the relative increase must be associated with excess resin which is introduced during the cylinder lay-up process.

As evidenced from Fig. 5, the thickness measurement is particularly useful in determining the exact location of overlaps, which may be required for numerical investigations. The thickness mapping may also be used to explain, in conjunction with imperfections and load eccentricities, any asymmetries or irregularities in the observed buckling mode. However, the reported thickness variations should be used carefully in comparative numerical or analytical studies as it is mainly due to excess resin. Owing to the relatively low elastic modulus

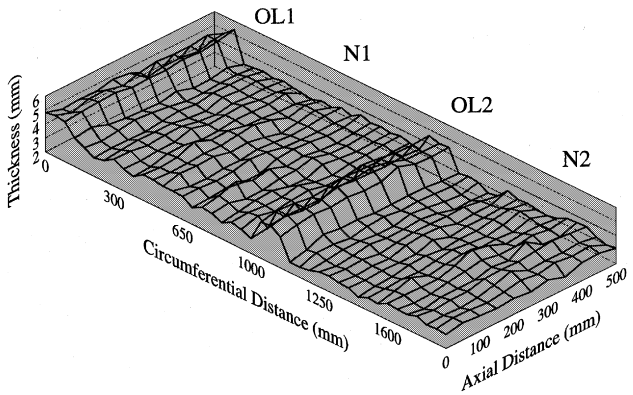

(a) Thickness measurement for RVM01 (0/0)

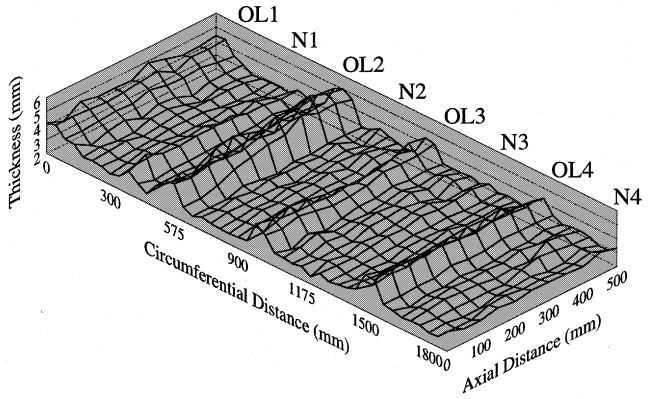

(b) Thickness measurement for RVM04 (0/90)

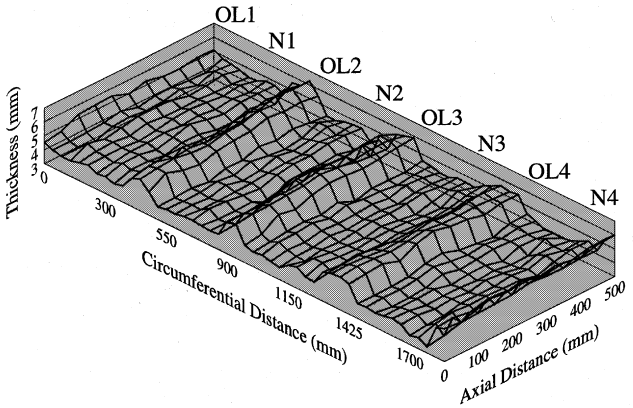

(c) Thickness measurement for RVM06 (0/90/0)

Fig. 5. Thickness measurement of cylinders: (a) RVM01 (0°/0°); (b) RVM04 (0°/90°); (c) RVM06 (0°/90°/0°).

compared to that of the fibres, possible variation in the overall laminate properties should be assessed.

5. Geometric imperfections

In view of the importance of initial geometric imperfections on the buckling behaviour of the cylinders, detailed measurement of these imperfections was undertaken. The automated laser scanning system was first used to obtain the imperfections of the specimen after it was mounted in the test rig and before any load was applied. The internal surface of the specimen was measured through a grid consisting of 31 axial stations (with an interval of 20 mm) and 72 circumferential stations (with an interval of 5° or 26.2 mm).

In order to generate a reference surface for the measurements taken on the specimen, the internal surface of an accurately machined steel ring with a diameter of 540 mm was also scanned at 5° intervals. The scan was undertaken at three vertical locations (100, 400 and 700 mm above the bottom platen) by bolting the steel ring on a set of three solid circular columns of corresponding heights. Thus, using these reference measurements, a datum for all imperfection and deflection measurements was created.

The 'raw' imperfection data were then processed using the so-called 'best fit' cylinder concept [10]. This concept accounts for possible misalignments between the longitudinal axes of the specimen and the measuring frame. Following the 'best fit' procedure, the resulting imperfections were analysed using two dimensional harmonic analysis to produce a set of Fourier coefficients. The advantage of this widely used data processing technique is that measured imperfections can be readily fed into analytical and numerical models. Furthermore, it facilitates comparative studies on the effect of the manufacturing process on the magnitude and spatial distribution of initial imperfections. It has been used successfully in previous imperfection measuring studies on composite shells [11]. In this testing programme, use was made of the following expression:

$$w_0(x,\theta) = \sum_{m=1}^{m_T}\sum_{n=0}^{n_T} \xi_{mn}\frac{m\pi x}{L}\sin(n\theta + \phi_{mn}), \qquad (1)$$

where $0 \leqslant x \leqslant L$ and $0 \leqslant \theta \leqslant 2\pi$, $w_0\ (x, \theta)$ is the initial imperfection function of the cylinder at any point, m the number of axial half waves, n the number of circumferential waves, and ξ_{mn} and ϕ_{mn} are the initial imperfection amplitude and phase angle associated with mode (m, n), respectively.

The imperfection surface was thus described by a set of coefficients, ξ_{mn} and ϕ_{mn}, with $m_T = 15$ and $n_T = 36$, these upper limits being determined from the number of readings taken axially and circumferentially. Eq. (1) represents a half range sine expansion in the axial direction, thus, imposing zero imperfection values at the two cylinder ends. The error introduced through this process is strictly confined to the end regions, with other parts of the Fourier expansion representing very closely the imperfection surface [8].

A full account of the imperfection measurements and generated Fourier parameters as well as a more detailed description of the data processing techniques are given elsewhere [8,12]. Fig. 6(a) shows a perspective view of

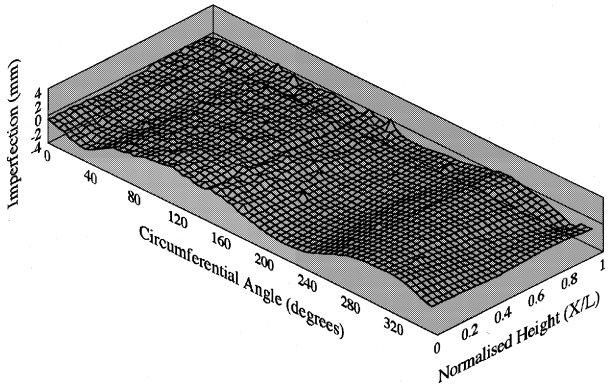

(a) Best-fit initial imperfectionsof Model RVM01

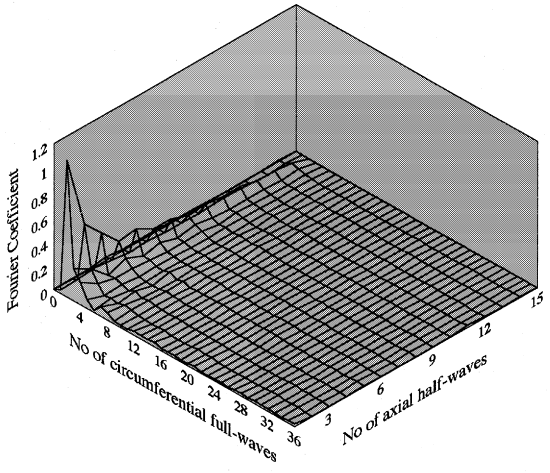

(b) Fourier coefficients of imperfections of Model RVM01

Fig. 6. (a) Best-fit initial imperfections of Model RVM01; (b) Fourier coefficients of imperfections for Model RVM01.

the 'best-fit' imperfection scan for Model RVM01, in which positive/negative values refer to outward/inward directions, respectively. A plot of the Fourier coefficients, as represented by Eq. (1) corresponding to the imperfection measurement of RVM01 is depicted in Fig. 6(b). The maximum imperfection amplitudes of all models, with the exception of the first Model RVM00 for which no measurement was taken, are presented in Table 4, together with the ratio of imperfection amplitude to nominal thickness. On the other hand, Table 5 summarises the three dominant modes (m, n) and the corresponding Fourier coefficients.

In general, the results indicate that dominant imperfection wavelengths along both the circumferential and the axial direction are ovalisation and barrelling, respectively, with maximum imperfection amplitudes being, on average, between 20% and 60% of the shell thickness. However, it should be noted that whereas lower imperfection modes exhibit high amplitudes, higher low-amplitude modes in both the axial and circumferential directions need to be adequately represented in analytical models as these could be more sympathetic to cylinder buckling modes under compression.

Table 4
Maximum imperfection amplitude for the test models

Model reference	Outward imperfection maximum amplitude		Inward imperfection maximum amplitude	
	w_0 (mm)	w_0/t	w_0 (mm)	w_0/t
RVM01	1.6	0.57	1.8	0.64
RVM02	1.7	0.61	1.0	0.36
RVM03	1.3	0.46	1.2	0.43
RVM04	1.3	0.46	1.5	0.53
RVM05	1.3	0.46	1.4	0.50
RVM05A	1.1	0.39	1.6	0.57
RVM05B	1.0	0.36	1.7	0.61
RVM06	0.9	0.21	1.0	0.24
RVM07	1.2	0.29	1.0	0.24

6. Buckling tests

6.1. Two-ply models with symmetric lay-up

The relationships between the total compressive load, applied by the actuator, versus the central axial shortening for all the 0°/0° models are depicted in Fig. 7. The first concentric test was carried out on Model RVM00 which was constructed from a two-ply laminate with a symmetric lay-up (i.e. 0°/0°). The test was primarily used as a pilot experiment to validate the set-up, particularly the arrangements of edge loads cells and transducers. Buckling occurred suddenly and audibly at 284 kN, with the load dropping to about half its value. Further increase in displacement caused a marginal increase in load.

The second concentric test on 0°/0° laminates was carried out on Cylinder RVM01. Buckling occurred suddenly at about 301 kN. Debonding and delaminations in the post-buckling range indicated the presence of some material damage, especially along the sharp edges of the buckles. Fig. 8(a) shows a perspective view of the laser scan of deflection taken directly after buckling, with positive values indicating outward deflection and negative values indicating inward deflection. As shown in the figure, buckling was spread over most of the circumference of the cylinder. All buckles were pronounced in an inward direction and the presence of the relatively stiffer overlap did not stop the buckles spreading across it. A view of the buckled shape of RVM01 is shown in Fig. 8(b). On unloading, the cylinder regained its original shape and most of its original stiffness. However, visual evidence of local delamination, through change of colour, was clearly present.

Table 5
Dominant Fourier coefficients and corresponding imperfection modes

Model reference	Dominant Fourier imperfection coefficients and corresponding modes					
	Fourier coeff. ξ_{mn} (mm)			Fourier modes (m, n)		
RVM01	1.13	0.52	0.37	(1,2)	(2,2)	(3,2)
RVM02	0.47	0.26	0.20	(1,2)	(2,2)	(3,2)
RVM03	0.56	0.38	0.27	(1,2)	(2,2)	(1,4)
RVM04	0.47	0.34	0.22	(2,2)	(1,2)	(1,4)
RVM05	0.60	0.44	0.31	(1,2)	(2,2)	(1,3)
RVM05A	0.58	0.27	0.25	(1,2)	(1,3)	(2,2)
RVM05B	0.55	0.41	0.22	(1,2)	(2,2)	(3,2)
RVM06	0.44	0.22	0.19	(1,2)	(2,2)	(1,4)
RVM07	0.29	0.23	0.12	(2,2)	(1,2)	(1,3)

For Cylinder RVM02, with a 0°/0° lay-up, the load was applied with an eccentricity of 30 mm from the centre representing an eccentricity-to-radius ratio (e/r) of about 0.1. The control load versus central end-shortening for this model is shown in Fig. 7(b). With a gradual increase in displacement, buckling occurred at a load of 291 kN, with the load suddenly dropping to about 161 kN. Failure was concentrated in the area under the eccentric load with one axial and three circumferential buckles towards the centre of the cylinder. Loading was continued in the post-buckling range and glass fibre rupture became evident accompanied by more delamination and debonding.

In Model RVM03, of 0°/0° lay-up, the eccentricity was increased to 75 mm (i.e. $e/r = 0.25$). The central load versus displacement relationship is shown in Fig. 7(b). Buckling occurred at a total load of about 260 kN. As in the previous test, one axial and three circumferential buckles were observed in the region of the applied load. In the post-buckling range, there was evidence of delamination and debonding principally in the circumferential direction with fibre rupture at the stiffened overlap.

6.2. Two-ply models with anti-symmetric lay-up

Using the same displacement-controlled loading regime described above, three concentric tests were carried out on Models RVM04, RVM05 and RVM05A, which had an anti-symmetric 0°/90° laminate lay-up. The load versus end-shortening relationships for the three cylinders are depicted in Fig. 9(a). Buckling occurred at 303, 283 and 290 kN, for RVM04, RVM05 and RVM05A, respectively. The behaviour of RVM04 and RVM05A was similar, with signs of delamination and material failure occurring only after buckling. On the other hand, buckling of Model RVM05 was preceded by delaminations and debonding which may explain the relatively lower strength, and possibly indicates manufacturing deficiencies in this model.

A full account of the pre and post-buckling wall deformations as measured from load cells and displacement transducers is given elsewhere ([12]). In some models, strain gauges were also placed to measure the axial and circumferential strains at mid-height of the specimen. For Model RVM05A, the average axial and circumferential strains at the point of buckling were about 0.3% (compressive) and 0.07% (tensile), respectively.

For Model RVM05B, the load was applied at an eccentricity of 75 mm (i.e. $e/r = 0.25$). The total load versus axial shortening at the centre of the cylinder is shown in Fig. 9(b). Buckling occurred at about 240 kN, with the load dropping to approximately 120 kN after buckling. The buckles were concentrated in the area of application of the eccentric load. At the point of buckling, and within the area of maximum stress, the peak axial strain was about 0.27%, and the circumferential strain was approximately 0.06%. In all the eccentric tests, the variation in load and displacement around the circumference of the specimen was accurately reflected in the measurements of edge load cells and corresponding transducers [12].

6.3. Concentric tests on three-ply cylinders

Two concentric tests were carried out on the three-ply 0°/90°/0° models (RVM06 and RVM07). The load-axial shortening relationships for these models are depicted in Fig. 10. As expected, failure occurred at a much higher load compared to previous models. For RVM06, failure occurred abruptly with a very loud noise at a load of 652 kN, and the cylinder lost almost all its load carrying capacity. Failure was sudden and evenly spread around most of the circumference of the cylinder. As the cylinder regained static equilibrium in the post-collapse region, there was no 'visible' sign of buckling deformation, but rather that associated with extensive material failure.

The behaviour of RVM07 was similar to RVM06, except that failure occurred at a relatively higher load. This was associated with more severe material failure distributed around almost the full middle cross-section of the cylinder. As shown in Fig. 10, the failure load was

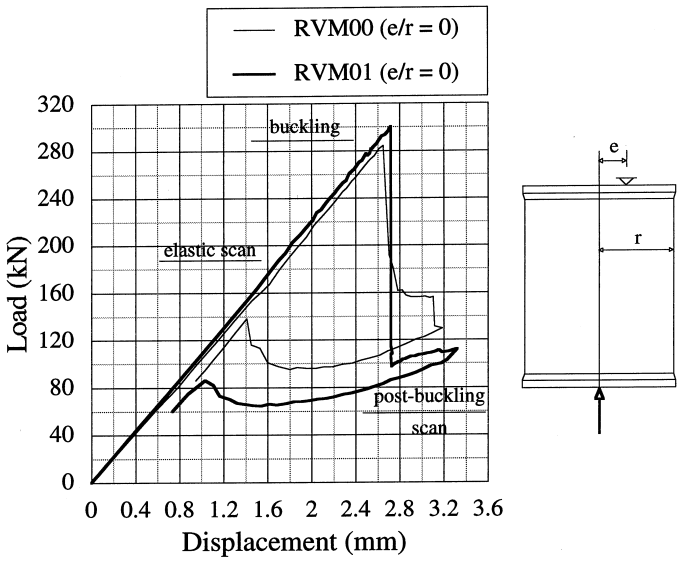

(a) Load-displacement relationship for concentric tests on 0/0 models (RVM00 and RVM01)

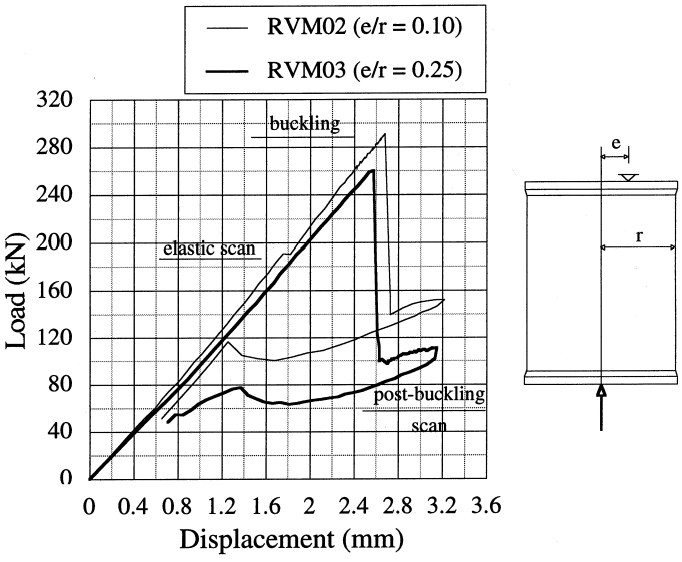

(b) Central load-displacement relationship for eccentric tests on 0/0 models (RVM02 and RVM03)

Fig. 7. (a) Load-displacement relationship for concentric tests on 0°/0° models (RVM00 and RVM01); (b) central load-displacement relationship for eccentric tests on 0°/0° models (RVM02 and RVM03).

about 704 kN, dropping sharply to about 20 kN. As in RVM06, failure was sudden and uniformly spread around the circumference of the cylinder. There was no visible sign of buckling deformation. Extensive material failure and complete breakage of fibres were clearly observed. A view of Model RVM07 after failure is shown in Fig. 11. At the peak load, the average axial and circumferential strains at the cylinder mid-height were 0.48% and 0.1%, respectively.

7. Discussion of results

7.1. Influence of thickness variation

As shown in Table 3 and discussed in Section 4 above, the average measured thickness of most cylinders is higher than the nominal value (specified as 1.4 mm per ply). In some cases, the increase in thickness is up to 20% compared to the specified nominal thickness,

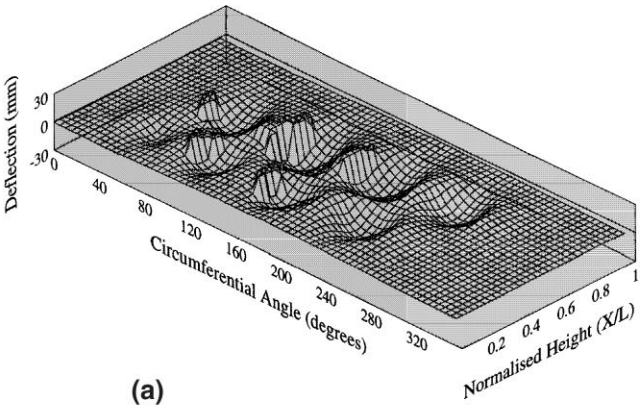

(a)

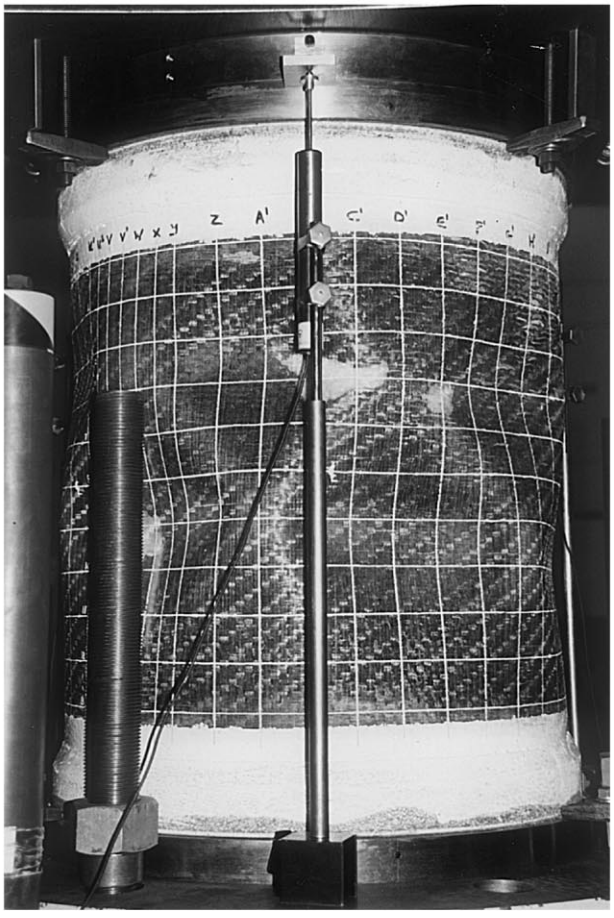

(b)

Fig. 8. (a) Post-buckling wall deformation scan of Model RVM01; (b) view of Model RVM01 after buckling.

excluding the effect of overlaps. This thickness variation is largely due to the excess resin introduced during the lay-up process of the models.

In analysis and design calculations, it is imperative that the relevant thickness used is a value, which for the ply thickness and laminate construction, gives the best correlation between analytical and experimental overall membrane, coupling and bending stiffnesses. Due to the important influence of thickness on buckling strength and mode, it is appropriate to adopt the actual measured thickness of the model. Nevertheless, the influence of any significant departure from the intended resin content, which the material properties are based on, should be adequately assessed.

The influence of resin content on material properties may be estimated by determining the change in the resin weight fraction, R. It can be shown ([13]) that the moduli E and G are directly influenced by the value of R. Within practical ranges, linear relationships may be assumed as follows

$$E^* = E\left(\frac{1-R^*}{1-R}\right) \quad \text{and} \quad G^* = G\left(\frac{1-R^*}{1-R}\right) \tag{2}$$

in which the superscript (*) refers to the modified property taking account of change of resin weight fraction from R to R^*. It is also assumed that the values of Poisson's ratios are virtually independent of R within its practical range.

Using Eq. (2), and the measured thickness of the models given in Table 3, the reduction in E and G values due to the increase in resin content may be estimated. For the two-ply models, it can be shown that an increase in thickness of 20% compared to the nominal thickness results in a reduction of E and G by more than 10%. However, since the material properties given in Table 1 are based on coupon specimens of thickness higher than the nominal (3.1 mm for the two-ply), the modification factors reduce to less than 6%. This could be considered as comparable to other variability sources which lead to an expected ±10% variability in the material properties.

Whereas it is important to use the actual measured thickness of the cylinders in numerical and analytical studies, it may be neither practical nor necessary to introduce relatively small changes in material properties particularly when the cylinder is represented by zones of different thickness as suggested in Section 4. Nevertheless, as discussed above, if the change in thickness is estimated to cause considerable variation in nominal material properties, such differences should be accounted for in analysis and design.

7.2. Axial stiffness

The axial load versus end-shortening plots depicted in Figs. 7, 9 and 10 give an indication of the experimental axial stiffness of the cylindrical models. For eccentrically-loaded models, a lower slope is observed as the plots shown represent the total load with respect to the shortening at the centre of the specimen. As expected, the axial stiffness of the three-ply models is considerably higher than that of the two-ply cylinders. It can also be observed that the axial stiffness of the 0°/0° and 0°/90° models is very similar, despite of the existence of coupling axial-bending terms in the stiffness matrix of the 0°/90° laminates.

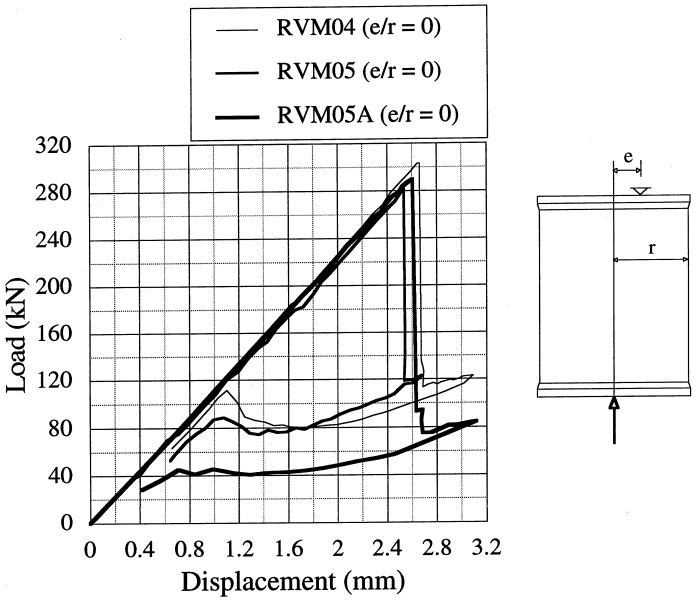

(a) Load-displacement relationships for concentric tests on 0/90 models (RVM04, RVM05, RVM05A)

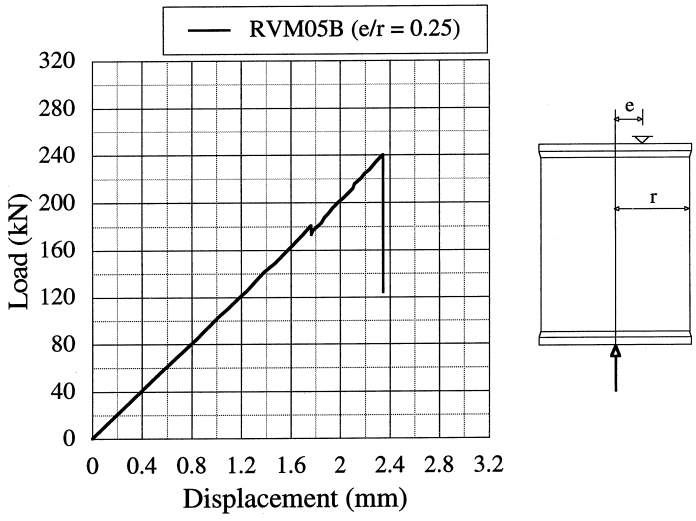

(b) Load-displacement relationships for the eccentric test on Model RVM05 B (0/90)

Fig. 9. (a) Load-displacement relationships for concentric tests on 0°/90° models (RVM04, RVM05, RVM05A); (b) load-displacement relationship for the eccentric test on. Model RVM05B (0°/90°).

In order to estimate the axial stiffness of the concentrically-loaded models, simplified analytical expressions may be used. The axial stiffness of a cylinder may be analytically estimated from the following relationship [14]:

$$N_x = \frac{E_x t}{(1 - v_{xy} v_{yx})} \left(\frac{\mathrm{d}u_o}{\mathrm{d}x} + v_{xy} \frac{w}{r} \right) \tag{3}$$

in which N_x is the axial load per circumferential length, w the radial displacement of the cylinder wall, r the radius to mid-surface of the cylinder, t the cylinder wall thickness and (E_x, v_{xy}, v_{yx}) are the apparent elastic properties of the laminate in the direction of the cylinder length.

Equation (3) is strictly applicable when the coupling terms in the stiffness matrices of the laminate are negligible. It can also be shown that the secondary term of the equation is insignificant for the laminates under consideration. Consequently, an estimate of the axial stiffness of the cylinder may be determined from the following expression:

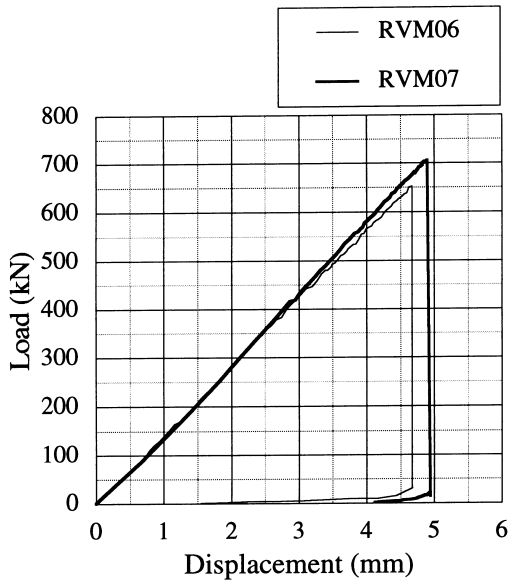

Fig. 10. Load-displacement relationships for the concentric tests on 0°/90°/0° cylinders (RVM06 and RVM07).

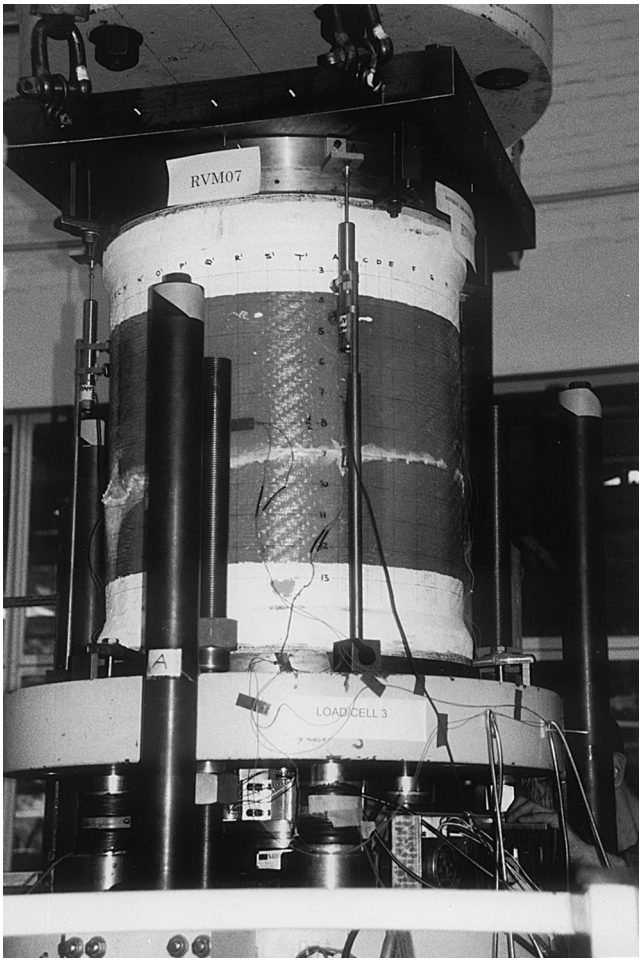

Fig. 11. View of Model RVM07 after failure.

$$k_x = \frac{E_x t}{(1 - v_{xy} v_{yx})} \tag{4}$$

in which k_x represents the normalised in-plane membrane stiffness for a unit circumferential and a unit axial length of the cylinder.

Based on Eq. (4), the membrane stiffness (in kN/mm) for the concentrically-loaded cylinders is estimated and compared to the experimental stiffness, as shown in Table 6. The apparent material properties in the axial direction of the cylinders were determined from classical laminate analysis based on the ply properties given in Table 1. The values of (E_x, v_{xy}, v_{yx}) adopted are (14.4 GPa, 0.26, 0.24), (13.8 GPa, 0.25, 0.25) and (14.0 GPa, 0.253, 0.246) for the 0°/0°, 0°/90° and 0°/90°/0° laminates, espectively. The average measured thickness of the models was used, but no account was taken of the influence of different resin contents on the apparent elastic moduli.

As indicated in Table 6, Eq. (4) appears to provide a reasonable upper bound estimate of the axial stiffness for most cylinders. The slight discrepancy between the analytical and experimental values may be attributed to several factors including variation in material properties, influence of resin content, effect of non-uniform thickness distribution and initial geometric imperfections. Further examination of these factors may be carried out using geometrically-non-linear numerical simulations.

7.3. Buckling strength

7.3.1. Experimental results

A summary of the experimental buckling loads of all cylinders is given in Table 7. As expected, whereas the 0°/0° and 0°/90° models exhibit similar buckling capacities, the strength of the three-ply models is more than two-fold. Moreover, whilst failure of the two-ply models is mainly by buckling, extensive material failure is associated with the behaviour of the three-ply cylinders. The ratio of the experimental buckling capacity to the axial material strength of the three-ply cylinders is approximately 40% compared to only 25% for the two-ply models. Consequently, material fracture in the three-ply cylinders occurs at relatively small post-buckling deformations, which are difficult to monitor experimentally. This interaction between buckling deformations and material failure requires further assessment using non-linear analysis in conjunction with appropriate failure criteria.

The influence of average model thickness on the experimental buckling strength may also be observed by comparing the behaviour of nominally-identical concentrically-loaded cylinders (e.g. RVM00 and RVM01, RVM06 and RVM07). With the exception of RVM05, the increase in thickness is associated with a relatively

Table 6
Experimental and analytical axial stiffness for concentrically-loaded cylinders

Model	Laminate	t (mm)	Stiffness (analytical) (kN/m)	Stiffness (test) (kN/mm)	Ratio (anal/test)
RVM00	0/0	3.18	115	108	1.06
RVM01	0/0	3.35	121	113	1.07
RVM04	0/0	3.15	111	114	0.98
RVM05	0/90	3.40	119	111	1.07
RVM05A	0/90	3.20	112	111	1.01
RVM06	0/90/0	4.35	154	143	1.08
RVM07	0/90/0	4.78	169	149	1.13

Table 7
Comparison between experimental strength and linear analysis

Specimen reference	Experim. load (kN)	Linear FE load (kN)	Ratio (exp/anal)
RVM00 (0°/0°, $e/r=0$)	284	428	0.66
RVM01 (0°/0°, $e/r=0$)	301	480	0.63
RVM02 (0°/0°, $e/r=0.1$)	291	445	0.65
RVM03 (0°/0°, $e/r=0.25$)	260	342	0.76
RVM04 (0°/90°, $e/r=0$)	303	426	0.71
RVM05 (0°/90°, $e/r=0$)	283	474	0.60
RVM05A (0°/90°, $e/r=0$)	290	426	0.68
RVM05B (0°/90°, $e/r=0.25$)	240	322	0.75
RVM06 (0°/90°/0°, $e/r=0$)	652	799	0.81
RVM07 (0°/90°/0°, $e/r=0$)	704	941	0.75

higher buckling strength. Although the increase in resin content leads to slightly reduced elastic moduli, it is evident that the effect of higher thickness on buckling strength is more pronounced.

In terms of load eccentricity, the behaviour of RVM02 indicates that an eccentricity of 10% (i.e. $e/r=0.1$) has a relatively insignificant influence on the buckling strength. The effect of such eccentricities appears to be of the same order of other inherent variabilties in the cylinders, particularly those related to variations in wall thickness as well as material properties. On the other hand, an eccentricity of 25% (i.e. $e/r=0.25$) causes noticeable reduction in the axial capacity of the cylinders as evidenced by the results of RVM03 and RVM05B.

7.3.2. Linear analysis

Estimates of the critical buckling strength of composite cylinders may be obtained using finite element analysis or through simple theoretical methods [14]. Both approaches provide comparable linear results, but the latter would usually impose some limitations in terms of laminate construction as well as boundary conditions. The finite element method forms a versatile method of analysis. Moreover, with due account of stiffness and geometric imperfections, detailed non-linear finite element analysis may be carried out to represent closely the buckling behaviour of the cylinders.

Preliminary analytical predictions were carried out in order to determine the linear buckling load of the cylinders. For this purpose, the Finite Element program ABAQUS [15] was used to estimate the buckling loads using linear eigen value analysis. This type of analysis does not account for non-linearities, and in particular the effect of initial geometric imperfections is not considered. The cylinder was modelled using 9-noded doubly curved shell elements (type S9R5), with 24 and 72 elements in the axial and circumferential directions, respectively. The material properties given in Table 1 were used in conjunction with the uniform wall thickness representing the average measured value. The parameters of the finite element model were determined following a number of benchmark and convergence studies carried out as part of the project [16].

The numerical linear buckling loads obtained for the cylinders are also given in Table 7. The same trends observed in the experimental results, in terms of the influence of number of plies, thickness variation and load eccentricity, are also generally reflected in the analytical values. It should be noted that, for simplicity, a uniform cylinder thickness was used in the analysis. By adopting the actual non-uniform thickness distribution, the eigen value results of some models can vary by up to 8%.

Based on the experimental and analytical results, the relative dependence of the buckling strength on the elastic moduli and the square of the wall thickness is observed. This is in general agreement with isotropic cylinders for which the theoretical critical buckling load, P_{cr} is given by:

$$P_{\mathrm{cr}} = \frac{2\pi E t^2}{\sqrt{3(1-\nu^2)}}, \tag{5}$$

where E and ν are Young's modulus and Poisson's ratio, respectively, for an isotropic material. Eq. (5) only applies to isotropic cylinders with idealised simply-supported end conditions, but it serves to highlight the dependence on elastic moduli and thickness. Analytical solutions for laminated orthotropic cylinders are also

available [14], but are predictably more complex due to the larger number of variables involved.

7.3.3. Knock-down factors

The ratio between the experimental buckling strengths and the linear buckling loads, presented in Table 7, gives and indication of the 'knock-down' factors for the cylinders. Knock-down factors are important for design purposes as they are used to reduce theoretical buckling predictions of nominal shells in order to account for the influence of imperfections and other unintended deviation from nominal values. In addition to the significant influence of initial geometric imperfections, other factors such as thickness variation, overlapping and load eccentricities would also affect these ratios.

As shown in Table 7, the ratio of experimental-to-linear buckling strength (i.e. knock-down factor) varies between 60% and 81% for all the cylinders. As pointed out before, this reduction in experimental strength is primarily due to the influence of initial geometric imperfections. As may be expected, the knock-down factors tend to increase with larger eccentricities as the role played by geometric imperfections becomes less important. This is evidenced by comparing the knock down factors of RVM03 and RVM05B to other concentrically-loaded two-ply models.

Knock-down factors also increase with the reduction in the cylinder radius-to-thickness slenderness. As shown in Table 7, the knock-down factor for the three-ply models (nominal $r/t = 72$) is, on average, about 20% higher than that of concentrically-loaded two-ply models (nominal $r/t = 108$). To this end, it may be useful to compare the results with the semi-empirical relationship for estimating the knock-down factor, α, used in the design of metal cylinders [17] given as:

$$\alpha = \frac{0.62}{1 + 0.0185(r/t)^{0.75}}. \tag{6}$$

Estimating the value of α for the two-ply and the three-ply models using Eq. (6), gives values of 0.38 and 0.43, respectively. These values are considerably lower that those based on the ratio of experimental-to-linear analysis results presented in Table 7. The above equation appears to provide a very conservative estimate of the knock-down factor for woven GFRP cylinders. However, experimental models are likely to produce higher values than real structures in view of their relatively simpler construction and controlled testing.

8. Concluding remarks

The results of buckling tests on GRP cylinders subjected to concentric and eccentric compression were presented in this paper. Particular attention was given to the measurement of imperfections and systematic data acquisition in order to provide data which may readily be used for validating analytical and numerical models. Some of the important conclusions and observations are summarised below.

(1) The manufacturing process of the cylinders, in this series hand lay-up, plays an important role in defining spatial thickness characteristics. In addition to the overlaps, significant thickness variations may exist within the normal zones of the models. Therefore, for adequate assessment of stiffness which would be necessary for analytical and numerical studies, accurate mapping of wall thickness should be undertaken.

(2) For some models, the average measured thickness was considerably higher than the nominal due to the extra resin introduced during manufacture. Whereas it is important to account for the actual measured thickness, the influence of departing from the nominal resin content on the effective material properties should be assessed. In general, the combination of thickness and material properties used in analysis and design calculations should represent the best correlation between analytical and experimental overall membrane, coupling and bending stiffnesses for the given laminate construction. Specimens taken from actual models should be examined in addition to standard characterisation tests.

(3) The automated laser scanning system provided an accurate and efficient non-contact technique for mapping the inner wall of the shell, particularly in terms of measuring the initial geometric imperfections. Dominant imperfection amplitudes were on average between 20% and 60% of the cylinder thickness. The laser scans provide information on manufacturing imperfections which, with appropriate statistical examination, may be used in codified specification of manufacturing tolerances.

(4) The axial stiffness of the three-ply models was about 30% higher than that of the two-ply cylinders. The 0°/0° and 0°/90° two-ply models exhibited almost the same stiffness largely due to the similarity between the material properties in the two directions. The experimental axial stiffness of the cylinders was in general agreement with predictions of simple analytical expressions based on the apparent material properties.

(5) Whereas failure of the two-ply models was dominated by elastic buckling, failure of the three-ply models was associated with significant material damage due to the relatively low radius-to-thickness ratio. This interaction between buckling and material failure warrants further analytical examination, through non-linear analysis.

(6) Variation in the average measured thickness of cylinders of the same laminate construction was shown to have a noticeable influence on the buckling strength. This appeared to be relatively more significant than the

effect of small load eccentricities ($e/r = 0.1$). When the eccentricity was increased to 25% (i.e. $r/t = 0.25$), the drop in axial capacity became pronounced, with a reduction of about 20%.

(7) Knock-down factors reflect the discrepancy between the experimental buckling strength and the linear theoretical prediction, primarily due to the influence of geometric imperfections. For the cylinders tested in this series, the estimated knock-down factors varied between 0.6 and 0.8. As expected, relatively high values are obtained for large load eccentricity or for low radius-to-thickness ratio, due to the reduced influence of imperfection in these situations.

(8) Based on a comparison with knock-down factors used for the design of metal shells, it appears that these factors provide a conservative estimate for the buckling strength of the woven GFRP cylinders examined in this study. With the availability of a more extensive database on laminated composite shells through detailed analytical studies supported by further experimental work, it may be possible to develop similar semi-empirical knock-down formulae. For the time being, it would appear that existing knock-down factors for axial compression may be used also for preliminary design of composite cylinders similar to those tested in this investigation.

Acknowledgements

The work presented in this paper was sponsored by the European Commission under a Brite-Euram programme (Project BE-7550: Design and Validation of Imperfection-Tolerant Shell Structures). Thanks are due to Intermarine-Spa for providing the specimens, to Prof. Poggi of Politecnico di Milano for carrying out material property tests, and to all the other partners for many productive discussions. The authors would also like to express their gratitude to Mr T Boxall and Mr R Millward of the Structures Laboratories at Imperial College for their dedication and professionalism in conducting the tests.

References

[1] Fung YC, Sechler EE. Thin-Shell Structures: Theory, Experiment and Design, New Jersey: Prentice-Hall, 1974.
[2] Jullien JF. Buckling of Shell Structures, on Land, in the Sea and in the Air, London/NewYork: Elsevier, 1994.
[3] Donnell LH, Wan CC. The effect of imperfections on buckling of thin cylinders and columns under axial compression. J. Appl. Mech. 1950;17;73–83.
[4] Koiter WT. The effect of axisymmetric imperfections on the buckling of cylindrical shells under axial compression. Proc. Kon. Ned. Ak. Wet. B 1975;6;265–270.
[5] Tennyson RC. Buckling of laminated composite cylinders: a review, Composites, January, 1975, 17–24.
[6] Simitses GJ, Shaw D, Sheinman I. Stability of imperfect laminated cylinders: A Comparison between Theory and Experiment. AIAA Journal 1985;23;1086–1092.
[7] Fuchs HP, Starnes Jr. JH, Hyer MW. Prebuckling and collapse response of thin-walled composite cylinders subjected to bending loads, In: Miravete A. (Ed.), Proceedings of the 9th Int. Conf. Comp. Mat. (ICCM-9), Vol. 1, Cambridge: Woodhead Publishing Co., 1993;410–417.
[8] Esong IE, Elghazouli AY, Chryssanthopoulos MK. Measurements Techniques for Buckling-Sensitive Composite Cylinders, Journal of Strain Measurement, February, 1998;11–18.
[9] Poggi C. Characterisation of materials, Brite-Euram Project: DEVILS, Report No. WP04.DR/PM(1), Italy: Politecnico di Milano, 1996.
[10] Arbocz J, Babcock CD. Prediction of buckling loads based on experimentally measured initial imperfections, In: Budiansky B. (Ed.), Buckling of Structures, Springer-Verlag, 1976;291–311.
[11] Chryssanthopoulos MK, Giavotto V, Poggi C. Characterization of manufacturing effects for buckling-sensitive composite cylinders. Composites Manufacturing 1995;6;93–101.
[12] Elghazouli AY. Esong IE, Chryssanthopoulos MK. Buckling Tests on GFRP Cylinders-Series I: Rovimat 1200, CESLIC Report OR 10, Imperial College, 1997.
[13] Smith CS. Design of Marine Structures in Composite Materials, Amsterdam: Elsevier, 1990.
[14] Vinson JR, Sierakowski RL. The Behaviour of Structures Composed of Composite Materials, Dordrecht: Kluwer Academic Publishers, 1987.
[15] ABAQUS. Theory and User's Manual, Hibbit, Karlsson and Sorensen, Providence, Rhode Island, 1995.
[16] Esong IE. Buckling Behaviour of Laminated GFRP Cylinders, PhD Thesis, Imperial College of Science, Technology and Medicine, London: University of London, 1999.
[17] Eurocode 3. Design of Steel Structures, Part 1-6: Supplementary Rules for the Strength and Stability of Shell Structures, ENV-1993-1-6, 1998.